Systematic errors in optical-flow velocimetry for turbulent flows and flames

Joseph Fielding, Marshall B. Long, Gabriel Fielding, and Masaharu Komiyama

Optical-flow (OF) velocimetry is based on extracting velocity information from two-dimensional scalar images and represents an unseeded alternative to particle-image velocimetry in turbulent flows. The performance of the technique is examined by direct comparison with simultaneous particle-image velocimetry in both an isothermal turbulent flow and a turbulent flame by use of acetone–OH laser-induced fluorescence. Two representative region-based correlation OF algorithms are applied to assess the general accuracy of the technique. Systematic discrepancies between particle-imaging velocimetry and OF velocimetry are identified with increasing distance from the center line, indicating potential limitations of the current OF techniques. Directional errors are present at all radial positions, with differences in excess of 10° being typical. An experimental measurement setup is described that allows the simultaneous measurement of Mie scattering from seed particles and laser-induced fluorescence on the same CCD camera at two distinct times for validation studies. © 2001 Optical Society of America

OCIS codes: 120.7250, 150.4620, 120.1740.

1. Introduction

The measurement of fluid velocity in reacting and nonreacting environments typically is accomplished by the tracking of particles that are seeded into the stream. Instantaneously evaluating multiple spatial components of velocity is possible by use of techniques such as laser Doppler velocimetry, particle-tracking velocimetry, or particle-imaging velocimetry (PIV). The drawbacks of using particle-based methods are practical complications that arise from introducing particulate material, which can obstruct flow or necessitate extensive cleaning, into gas-handling systems. Additionally, although it has been demonstrated that PIV can be combined with scalar measurements by use of laser-induced fluorescence (LIF),[1] Lorenz–Mie scattering from the seed particles interferes with simultaneous diagnostics at or near the laser wavelength. This interference is especially problematic for imaging Rayleigh scattering, which is an important measurement for mixture-fraction determination in turbulent nonpremixed flames.[2–4]

Alternative nonparticle approaches have been applied to turbulent combustion environments, a number of which can broadly be classified as optical-flow (OF) velocimetry techniques. Here we use the term to encompass any approach that relies on continuous scalar images (as opposed to discrete particle images) for velocity information. OF is the apparent motion of the brightness or the intensity pattern in an image pair or sequence.[5] OF is distinct from *image* flow, which is defined as the two-dimensional (2-D) projection of the instantaneous three-dimensional velocity of a point on the image plane.[6] It is possible to have image flow without OF, as in the case of a patternless rotating sphere; the absence of a pattern results in the absence of a spatial gradient. It is clear, then, that image regions that lack sufficient variation in scalar intensity will cause problems because OF algorithms will produce incorrect velocities in these regions. This condition of inhomogeneity should not present difficulties in turbulent flows as long as the measured scalar field exhibits resolvable spatial gradients.

It can be shown that the component of the image flow that is normal to the brightness gradient is equal to the component of the OF that is normal to the brightness gradient under certain conditions, including spatiotemporally uniform lighting.[6] It is common in the computer-vision literature to assume that

J. Fielding and M. B. Long (marshall.long@yale.edu) are with the Center for Laser Diagnostics, Department of Mechanical Engineering, Yale University, New Haven, Connecticut 06520-8284. G. Fielding is with the Imaging Science Division, Eastman Kodak Company, Rochester, New York 14650. M. Komiyama is with the Department of Mechanical Engineering, Osaka University, Osaka, Japan.

Received 15 May 2000; revised manuscript received 14 September 2000.

0003-6935/01/060757-08$15.00/0

the two flow fields are equivalent.[7] For fluid motion the assumption is valid when the velocity in the third, unmeasured direction is small or the scalar gradient in that dimension is small.[8] Other restrictions exist for using OF algorithms for velocimetry applications, such as consistency between frames. Large interframe times can be problematic for fast flows if the pixel displacements are too large.

OF algorithms are generally broken down into categories that are based on differential techniques, region-based matching, and frequency methods; a review of these approaches can be found in Ref. 9. The image-correlation velocimetry technique of Tokumaru and Dimotakis[8] provides a framework for measuring the displacement fields of fluid motions. Extension of this approach to reacting flows appears to be feasible,[10,11] provided that appropriate scalars are imaged and the algorithms are validated experimentally. The scalar imaging velocimetry approach of Dahm *et al.*[12] produces a velocity field by the inversion of the scalar transport equation—an approach that has been applied to large Schmidt number flows—but four-dimensional data sets are required. Specific OF algorithms were already examined for their potential to increase the accuracy of velocities obtained from PIV.[13] Related work in OF validation is currently underway by use of experimental techniques that are similar to those presented in this paper.[14,15] Limited test cases are examined, and often the error is defined based on the difference between mean velocity fields rather than on an ensemble average of instantaneous errors. Such an approach will underrespresent the actual error of the OF.

In this paper, we compare velocities obtained from PIV and from exemplar OF algorithms that are applied to scalar image pairs. Two experimental configurations are described that involve the simultaneous measurement of Lorenz–Mie scattering from seed particles and the LIF of acetone or acetone–OH. In one setup all quantities were imaged with a single dual-frame CCD camera, eliminating errors that are due to differing system resolutions. Both arrangements allow for the determination of velocity from cross-correlation PIV and OF from scalar image pairs; results are presented for reacting and nonreacting flows.

The OF algorithms used in the present study are both region-based techniques that produce velocities by the choice of the displacement with the maximum correlation coefficient on the basis of matching spatial features within a specified search window. Anandan[16,17] developed a method for computing dense (i.e., 100% image coverage) OF fields from a pair of images. The method uses a hierarchical-matching approach to refine matches to subpixel resolution. The key elements of the flow algorithm are (i) the match criterion, (ii) the confidence measure, (iii) the smoothness constraint, and (iv) the control strategy. The algorithm begins by the creation of a Laplacian pyramid for each of two input images in which the levels are composed of subsampled images and the zero level contains the full-resolution image. The match criterion for every pixel is the minimization of a Gaussian-weighted sum-of-squared differences (SSD) correlation measure. An $N \times N$ window is used to compute the SSD for all potential matches within a particular radius of the chosen pixel and at every level.

Although the original implementation of Anandan's research suggests a 5×5 kernel for each level of the pyramid, we chose to make the size of the Gaussian kernel N a function of the pyramid level. The reason is that, at low levels in the pyramid (finer images), we may want a larger correlation region. However, at higher levels in the pyramid (coarser images) the correlation region should be smaller because each pixel spans a larger area. Because of the dyadic scaling between levels, we chose the following rule for determining N: $N = \max[K/(\text{level} + 1), 5]$, where K is a parameter (we use $K = 15$ for all examples in this paper). A 3×3 region around the best match within the set of candidate matches is used to create the SSD surface. The principal axes corresponding to the principal curvatures are computed after fitting a quadratic surface to the data by use of a technique developed by Beaudet.[18] Confidence measures of the flow estimates are used to guide the implementation of the smoothness constraints, which helps to generate smooth displacement fields, and an iterative relaxation algorithm is used to update the flow field. Finally, a control strategy guides the optimization as it proceeds from the coarsest level on the resolution pyramid to the finest resolution. In this paper, we refer to the present implementation of this algorithm as F-OF for purposes of brevity.

The second OF algorithm employed was developed by Komiyama *et al.*[10] and is applied to both scalar and particle images for velocimetry purposes. This technique differs from F-OF with respect to the control strategy, and cross-correlation surfaces are computed for the full-resolution image within a specified search window. For this study the search window has a fixed dimension: a width of 31 pixels (centered on the search pixel) and a height of 32 pixels (in the positive y direction). The size of the reference matrix (or the interrogation region) can be varied as needed to handle the image resolution and the signal-to-noise ratio (SNR). A smoothness constraint can be applied to the computed velocities in the form of a 3×3 Gaussian filter. The same cross-correlation algorithm is used for PIV, giving results that are comparable with frequency-based methods (the 2-D fast Fourier transform), although at increased computational cost. In subsequent sections, we refer to this technique as K-OF.

2. Experiment

Figure 1 shows the first configuration (setup A) that was used for acetone LIF and PIV. The fourth harmonic (266 nm) of a double-pulsed Nd:YAG laser (Continuum, Model Powerlite 8000) illuminates seed particles for PIV and excites acetone fluorescence for scalar imaging. The beam passes through a cylin-

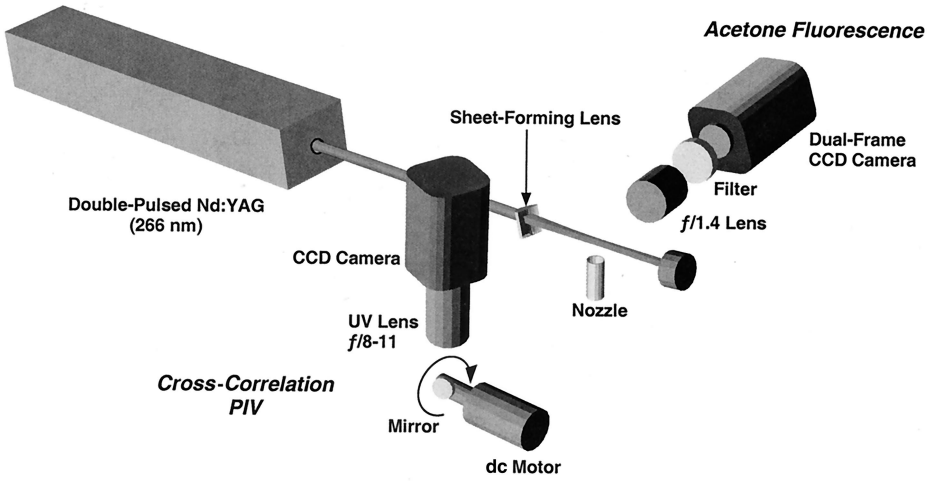

Fig. 1. Experimental setup A used for simultaneous acetone LIF and PIV measurements in nonreacting flows.

drical quartz lens with a 300-mm focal length, forming a sheet approximately 5 mm in height with a beam waist of 200 μm. The interpulse time of 32 μs gives an energy of approximately 1.0 mJ/pulse. Micrometer-sized sugar particles are introduced into the air flow by use of an aerosol seeder (TSI, Model 9306). A fraction of the air flow is passed through a heated bubbler unit consisting of a porous tube that is submerged in acetone. The nozzle used for this particular configuration is a straight tube with 4.57-mm inner diameter. The turbulent isothermal air jet issues into an unconfined low-velocity coflow of air (2.6 m/s). The results presented here correspond to a jet with a Reynold's number of Re = 2810 and an exit velocity of 7.7 m/s.

Lorenz–Mie scattering from the particles is collected by use of an $f/11$ quartz camera objective (Nikon, Model Nikkor UV) coupled to a liquid-cooled UV-sensitive (a quantum efficiency of 10%) CCD camera (Photometrics, Model CH350). A UV-enhanced mirror with an aluminum front surface is mounted to a dc motor rotating at approximately 50 Hz to separate the two pulses spatially from the laser on the 2000 × 2000 pixel CCD. The timing of the experiment is controlled by the reflection of a He–Ne laser from the mirror onto a photodiode to trigger the laser electronics and synchronize the cycle.

Broadband acetone fluorescence occurs between 350 and 550 nm, which makes unintensified imaging possible. Fluorescence from the two laser pulses is imaged by use of an interline-transfer CCD camera (PCO/Cooke Corporation, Model SensiCam) coupled with a large-format $f/1.4$ camera objective. This camera allows the acquisition of two images that are temporally separated by at least 1 μs. A clear glass filter (Schott, Model WG305) is used to block residual Mie scattering.

The optical configuration provides 54 pixels/mm for the particle image and 36 pixels/mm for the scalar image. Using separate cameras to capture scalar and particle images introduces experimental uncertainties as a result of differing resolutions and registrations, as does mechanical jitter in the timing of the mirror rotation. Here the uncertainty in the PIV measurements is conservatively estimated to be ±1 pixel in the y direction, corresponding to a velocity uncertainty of ±0.3 m/s.

The second experiment effectively eliminates the uncertainty by the detection of both frames on the CCD chip of a single dual-frame camera by use of a split-mirror configuration. Figure 2 shows the arrangement (setup B) of this experiment. Light is collected with a quartz camera objective (Nikon, Model Nikkor UV; $f/4.5$) and directed onto two front-surface mirrors to split the image before coming to focus on the fast-phosphor image intensifier (Delft

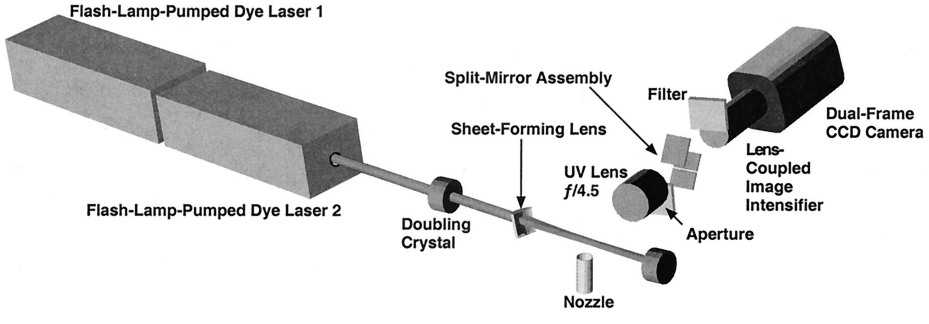

Fig. 2. Experimental setup B use for simultaneous acetone–OH LIF and PIV measurements in reacting flows.

Electronic Products, Model XX1450RT). The camera is lens coupled to the image intensifier with matching $f/1.4$ camera objectives. Two flash-lamp-pumped dye lasers (Candela, Model LFDL-20) are combined to form a single laser with independently controlled amplifiers (Pyrromethene 567, 2.2×10^{-5}M in methanol). The three-prism tuner is aligned by use of the output of a Nd:YAG-pumped dye laser (Continuum, Model ND6000) tuned to 563.88 nm. This wavelength is chosen such that the frequency-doubled output (281.94 nm) of the dye laser coincides with overlapping rotational–vibrational transitions in the A–X electronic transition of the OH radical centered on $Q_1(1)$. This relation is significant in that it allows the simultaneous visualization of acetone and OH LIF in a flame, creating a more continual scalar field than does acetone alone, which disappears when approaching the flame front.

The fundamental of the laser is doubled through a BBO crystal, filtered to reject residual visible light, and focused by a cylindrical quartz lens (300-mm focal length) into a sheet approximately 6 mm high with a beam waist of ~400 μm. The wavelength-conversion efficiency for the system is modest at an interpulse time of 25 μs, generating only 1 mJ/pulse in the UV for approximately 500 mJ/pulse in the visible. Higher energies are possible with longer pulse separations, as the dye in the second cell has more time to recover from the first pulse of the laser.

The burner used for this configuration consists of a 6.1-mm-diameter nozzle surrounded by a 14-mm-diameter pilot-flame region. N_2 is used in the acetone bubbler to reduce flame luminosity and soot, and 1-μm alumina particles are injected through an air-fed cyclone seeder. The turbulent flame that results is a premixture of acetone, N_2, and air that is stabilized by a methane–air pilot flame. There is a large degree of local extinction because of the high-velocity air coflow (~6 m/s). The results presented correspond to a Re = 3500 jet with an exit velocity of 7 m/s, and imaging was performed 67 mm downstream of the nozzle exit.

3. Error and Confidence Measures

With simultaneous PIV information it is possible to calculate the error in the computed OF velocity field. This error can be expressed in a number of ways to quantify the performance of a particular OF algorithm for velocimetry. The first measure can be written as

$$\mathbf{V}_e = \frac{1}{N}\sum_{i=1}^{N}|\mathbf{V}_P - \mathbf{V}_{OF}|, \tag{1}$$

where $\mathbf{V}_P$ and $\mathbf{V}_{OF}$ are the PIV and the OF velocity fields, respectively, for image i and the summation is performed over N images. Additionally, it is useful to examine an expression that is based on angular differences

$$\theta_e = \frac{1}{N}\sum_{i=1}^{N}|\theta_p - \theta_{OF}|, \tag{2}$$

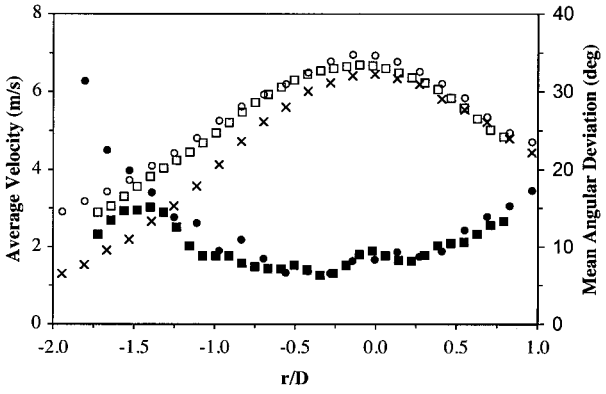

Fig. 3. Mean velocities [PIV (×), F-OF (○), K-OF (□)] and angular deviations [F-OF (●), K-OF (■)] for the case of a nonreacting flow as measured by setup A and plotted as a function of the radial position r/D.

where θ is the orientation of the vector considered.

It is also useful to examine confidence measures that, in the absence of *a priori* knowledge of the velocity field, could be used to indicate the accuracy of the local OF estimate. Anandan[16] proposed using the curvature of the SSD surface, which is used in the control strategy for replacing low-confidence flow estimates. In the most general sense the topography of the correlation map qualitatively describes the exactness of a potential match point. As is demonstrated below, discrete particle images result in sharp correlation peaks, whereas continuous scalar images create broad ridgelike structures that are associated with the motion of edges between frames.

4. Results

The mean velocity computed in three different ways from an ensemble of 50 images (setup A, nonreacting flow) is displayed in Fig. 3 as a function of radial location. The ensemble-averaged angular deviation, which was computed with Eq. (2), between the instantaneous PIV and OF vectors is also shown. Immediately apparent from the figure are the systematic errors in the computed OF velocity magnitudes and directions with increasing distance from the center line.

Figure 4 displays the mean-difference velocity [computed from Eq. (1)] scaled by the local velocity obtained from PIV. This representation indicates errors of approximately 25% at the center line that increase to more than 75% at the edges ($r/D \sim 1.5$).

It is true that the fluorescence intensity decreases with increased r/D on a mean basis and that, consequently, the local mean SNR is reduced. However, mean scalar cross-correlation values for K-OF do not indicate any decrease with radial position, as might be expected if a low SNR were the cause for the systematic errors. It is more likely that increased scalar homogeneity and the increasing spatial scale of the structures appearing at the edges of the image pairs result in the incorrect velocity displacements and directions. Indeed, varying the resolution of the

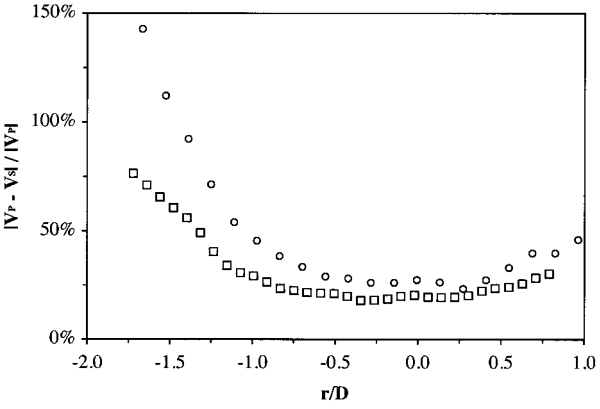

Fig. 4. Mean-difference velocity [F-OF (○), K-OF (□)] computed with expression (1) and displayed as a percentage of the local mean PIV velocity magnitude for the case of a nonreacting flow as measured with setup A.

OF algorithm changes the magnitude of the angular deviations most significantly at larger r/D. In Fig. 4 the K-OF shows the smallest mean deviation obtained with a 127 × 127 pixel reference matrix (the size used for the curves shown in Figs. 3 and 4). The F-OF algorithm produces larger deviations on a mean basis, especially away from the center line, but uses smaller effective reference windows (roughly 15 × 15 pixels at full resolution). Increasing the reference-window size for the F-OF produces little advantage, as is the case with the K-OF, probably because of the hierearchical-matching scheme employed. For the present experimental data larger correlation regions appear to be more favorable in terms of reducing angular errors with consequent reductions in the spatial resolution.

Figure 5 presents a representative scalar image pair from the nonreacting turbulent jet, and Fig. 6 shows the associated velocity vectors. Vectors are shown every 0.37 mm for PIV, the K-OF, and the

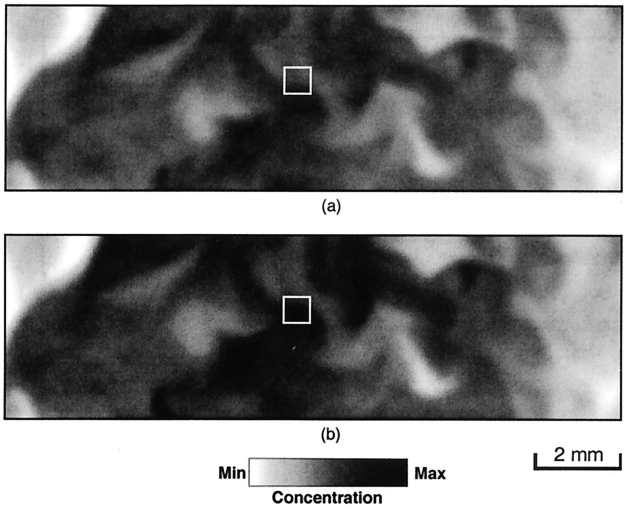

Fig. 5. Scalar fluorescence images shown at two times: (a) t_0 and (b) t_0 + 57 μs. The white-outlined boxes correspond to the regions used for Fig. 7.

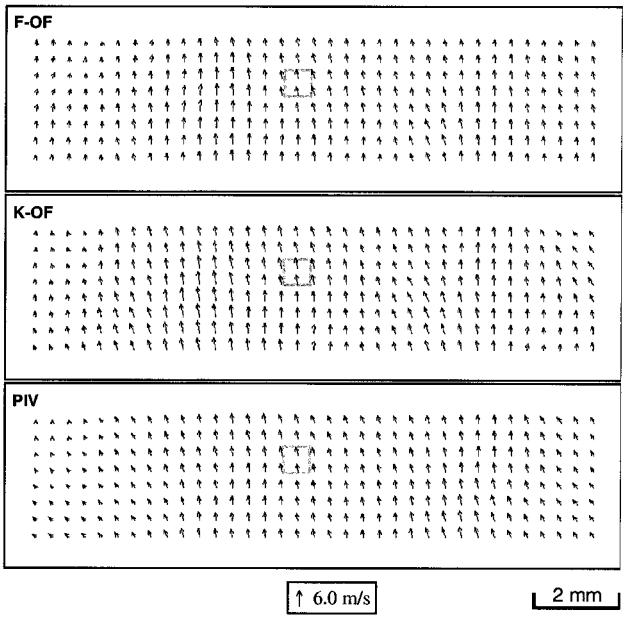

Fig. 6. Results of the F-OF, the K-OF, and the PIV vector-field determinations. The boxes indicate the regions used for Fig. 7.

F-OF. The boxes drawn in the frames of the scalar and the vector fields represent the search window used for the K-OF, and the correlation maps for that window are shown in Fig. 7. The contours represent 10% increments between the minimum and the maximum values; the inner contour represents 90% of the maximum correlation value. These correlation maps underscore the qualitative difference between operating on discrete and continuous images for velocity determination. In Fig. 7(a) a distinct cross-correlation peak is shown for the discrete particle image pair. For the scalar image pair a correlation surface is formed [Fig. 7(b)] from which it is apparent that the physical dimension of the peak region is larger than that for the discrete particle case. Smaller reference windows result in broader peaks if the intensity variation within that window becomes more homogeneous as a result. Similar surfaces can be drawn for the F-OF, and a more detailed discussion of SSD maps is found in Ref. 16.

For the reacting-flow case (setup B) Figs. 8 and 9 show the mean velocities, the mean angular deviations, and the mean-difference velocities computed from an ensemble of 30 images. The velocity magnitudes show the correct qualitative trends, but angular errors are significant with center line values of ~10° for both OF algorithms. The errors again increase toward the image edges. Overall, the mean angular deviations for the F-OF algorithm appear to be lower than those for the nonreacting case, despite the lower SNR for the scalar image pairs compared with the previous experiment. This result may be attributed in part to the increased laser-sheet thickness, which can attenuate the effect of out-of-plane motion of isoscalar surfaces.

Figure 10 shows a scalar image pair for the flame,

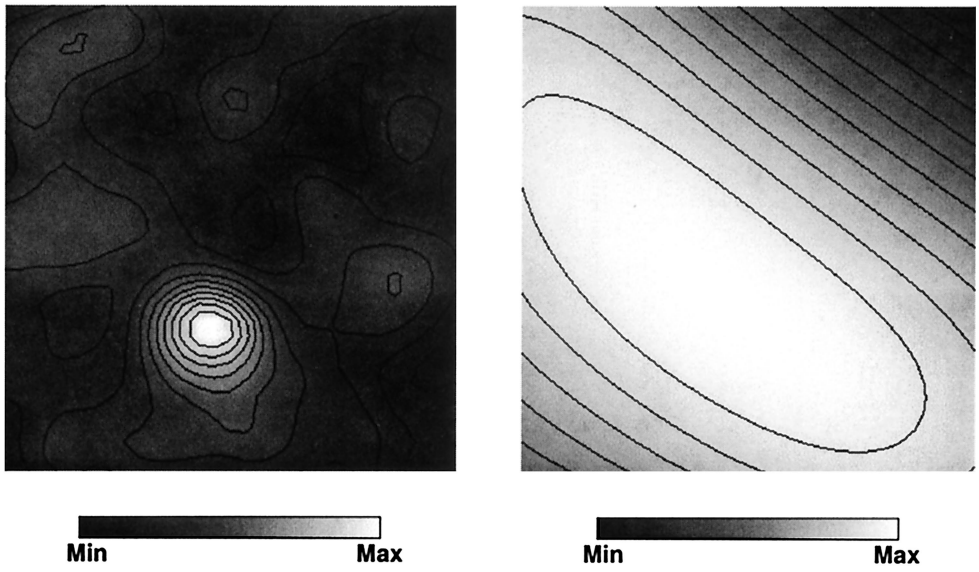

Fig. 7. Correlation maps for the regions indicated by the boxes in Figs. 5 and 6: (a) the PIV map showing a discrete peak and (b) the broader ridgelike feature of the K-OF.

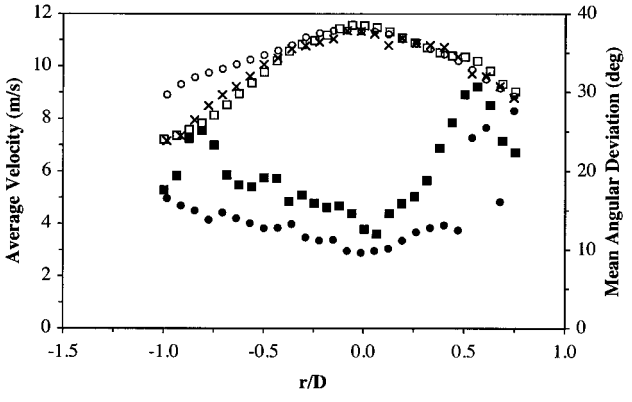

Fig. 8. Mean velocities [PIV (×), F-OF (○), K-OF (□)] and angular deviations [F-OF (●), K-OF (■)] for the case of a reacting flow as measured by setup B and plotted as a function of the radial position r/D.

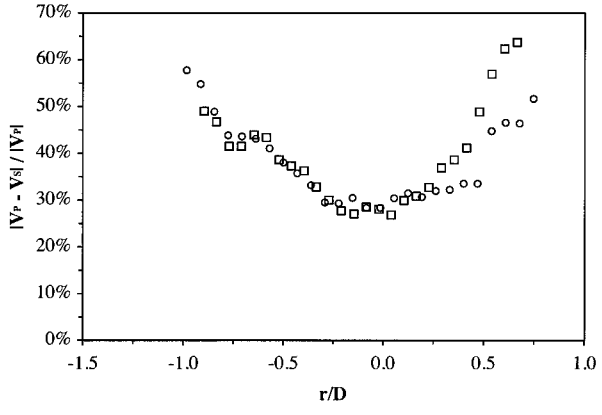

Fig. 9. Mean-difference velocity [F-OF (○), K-OF (□)] computed with expression (1) and displayed as a percentage of the local mean PIV velocity magnitude for the case of a reacting flow as measured with setup B.

which shows the inner turbulent jet of acetone as well as the presence of OH toward the flame zone. Disappearance of the acetone as a result of pyrolysis prior to the flame zone is evident from the figure and must to some extent contribute to the overall velocity error measured with OF velocimetry. The laminarization of the flow with local heat release poses a problem for the application of OF techniques to reacting flows in that many scalar quantities will ap-

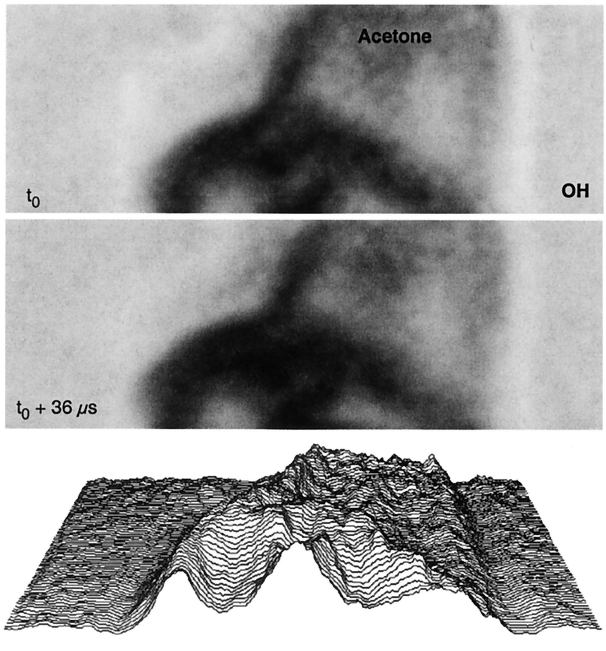

Fig. 10. Scalar fluorescence images for the flame case with regions of OH and acetone marked. The surface plot indicates the relatively weak OH florescence signal, which results from the broad linewidth of the pump laser.

pear to be homogeneous as a result, such as the OH field in Fig. 10.

Moreover, the alignment of the scalar field being imaged is a significant factor in the success of OF velocimetry, a fact that is recognized in the discussion of Ref. 19. Note that, in Fig. 10, the imaged scalar interface is aligned with the flow direction (here, vertically) where the flame is located. Vertical displacement of a vertically oriented line, for example, is resolvable only if horizontal edge features appear within both frames of the reference window. In general, translational motion of an edge allows unique determination of the velocity component in only the gradient direction. This describes the classical *aperture* problem of OF and represents an obstacle to the use of continuous scalar fields for velocimetry. This obstacle might be overcome in part by use of a larger reference window with a commensurate decrease in the spatial resolution of the vectors.

5. Conclusions

Simultaneous OF velocimetry and PIV have been demonstrated for reacting and nonreacting turbulent jets by use of two experimental configurations. The data presented indicate systematic angular discrepancies on a mean basis with increases evident with distance from the flow center line. Two representative OF algorithms have been considered; they produced differing numerical results for the velocity magnitude and direction but exhibited the same trends.

Noise is ruled out as the cause for these systematic angular errors on the basis of the behavior of the correlation coefficients; no decrease in the correlation value is observed with increasing r/D. More likely, the disagreement arises from a combination of the maximum local scalar gradient's aligning with the direction of motion (in the reacting case) and the dimensions of such features' exceeding the reference-window size—the so-called aperture problem. A low SNR in the scalar images is generally undesirable because it might affect the exact displacement match that is associated with the broad peak region (compared with PIV) shown in the correlation topography for the search window. Another important factor to be considered is the thickness of the laser sheet used in scalar imaging for OF. Large out-of-plane motion of an isoscalar surface will cause errors in OF velocimetry that will be exacerbated for thin laser sheets. The condition is more restrictive for OF velocimetry than for PIV owing to the continuous nature of the scalar images. Three-dimensional OF velocity measurements with two or three spatially separated laser sheets could be employed to address this issue.

Correlation maps such as those shown in Fig. 7 suggest that confidence in the velocity determined by OF techniques could be related to the pixel dimension of the correlation peak within some specified tolerance of the maximum value (i.e., the match point). At present, however, this hypothesis is not borne out by the data. Broad physical peak regions with correspondingly large correlation coefficients do not necessarily imply erroneous OF velocities on an instantaneous basis. It is difficult to quantify the uncertainties more accurately because the topology of the correlation maps can vary dramatically from region to region in the image pair, depending on the size and the number of resolvable features within the reference window. There is a relation between the correlation-peak size and the velocity error when the data are conditionally sampled according to radial location—larger r/D show both larger errors and increased correlation-peak size, suggesting that changing spatial scales are partly responsible for the effect.

Selective filtering of spatial scales within the reference window might prove to be more valuable for establishing a confidence measure. For any OF algorithm the confidence measure is a necessary component for velocimetry in turbulent systems to place proper limits on the uncertainty associated with the measurement. Overall, the present study has indicated that OF has limitations for application to gas-phase reacting and nonreacting flows. On a single-shot basis the OF algorithms considered here produce results that are in only approximate agreement with PIV. However, on a mean basis, systematic errors become evident, and these must be addressed in ongoing studies of this technique.

Other OF algorithms exist that span a wide range of computational methodologies. Some may produce different results from the data than do the algorithms described in this paper. Combining the most successful and robust features of the approaches might address issues that have been raised by the present study. For this reason the scalar and the particle image pairs described in this paper are available in tagged image file format.[20]

References

1. J. H. Frank, K. M. Lyons, and M. B. Long, "Simultaneous scalar–velocity field measurements in turbulent gas-phase flows," Combust. Flame **107,** 1–12 (1996).
2. S. H. Stårner, R. W. Bilger, M. B. Long, J. H. Frank, and D. F. Marran, "Scalar dissipation measurements in turbulent jet diffusion flames of air diluted methane and hydrogen," Combust. Sci. Technol. **129,** 141–163 (1997).
3. J. Fielding, A. M. Schaffer, and M. B. Long, "Three-scalar imaging in turbulent nonpremixed flames of methane," in *Proceedings of the Twenty-Seventh International Symposium on Combustion* (The Combustion Institute, Pittsburgh, Pa., 1998), pp. 1007–1014.
4. S. H. Stårner, R. W. Bilger, K. M. Lyons, J. H. Frank, and M. B. Long, "Conserved scalar measurements in turbulent diffusion flames by a Raman and Rayleigh ribbon imaging method," Combust. Flame **99,** 347–354 (1994).
5. B. K. P. Horn and B. G. Schunk, "Determination of optical flow," Memo 572 (Artificial Intelligence Laboratory, MIT, Cambridge, Mass., 1980).
6. A. Singh, *Optic Flow Computation: A Unified Perspective* (IEEE Computer Society, Los Alamitos, Calif., 1990).
7. A. M. Waxman and J. H. Duncan, "Binocular image flows: steps toward stereo-motion fusion," PAMI **8,** 715–729 (1986).
8. P. T. Tokumaru and P. E. Dimotakis, "Image correlation velocimetry," Exp. Fluids **19,** 1–15 (1995).
9. J. L. Barron, D. J. Fleet, and S. S. Beauchemin, "Performance

of optical flow techniques," Int. J. Comput. Vision **12,** 43–77 (1994).
10. M. Komiyama, A. Miyafuji, and T. Takagi, "Flamelet behavior in a turbulent diffusion flame measured by Rayleigh scattering image velocimetry," in *Proceedings of the Twenty-Sixth International Symposium on Combustion* (The Combustion Institute, Pittsburgh, Pa., 1996), pp. 339–346.
11. G. Grünefeld, A. Graber, A. Diekmann, S. Krüger, and P. Andresen, "Measurement system for simultaneous species densities, temperature, and velocity double-pulse measurements in turbulent hydrogen flames," Combust. Sci. Technol. **135,** 135–152 (1998).
12. W. J. A. Dahm, L. K. Su, and K. B. Southerland, "A scalar imaging velocimetry technique for fully resolved four-dimensional vector velocity field measurement in turbulent flows," Phys. Fluids A **4,** 2191–2206 (1992).
13. G. M. Quénot, J. Pakleza, and T. A. Kowalewski, "Particle image velocimetry with optical flow," Exp. Fluids **25,** 177–189 (1998).
14. G. Grünefeld, J. Bartelheimer, H. Finke, and S. Krüger, "Application of gaseous image velocimetry to laminar, unsteady flames," in *Proceedings of the Seventeenth International Colloquium on the Dynamics of Explosions and Reactive Systems* (Interdisziplinäres Zentrum für Wissenschaftliches Rechnan, University of Heidelburg, Heidelburg, Germany, 1999), Paper no. 184.
15. G. Grünefeld, J. Bartelheimer, H. Finke, and S. Krüger, "Gas-phase velocity field measurement in sprays without particle seeding," Exp. Fluids **29,** 238–246 (2000).
16. P. Anandan, "Measuring visual motion from image sequences," Ph.D. dissertation (Department of Computer and Information Science, University of Massachusetts, Amherst, Mass., 1987).
17. P. Anandan, "A computational framework and an algorithm for the measurement of visual motion," Int. J. Comput. Vision **2,** 283–310 (1989).
18. P. R. Beaudet, "Rotationally invariant image operators," Proc. Int. Conf. Patt. Recog. 579–583 (1978).
19. A. J. Pearlstein and B. N. Carpenter, "On the determination of solenoidal or compressible velocity fields from measurements of passive or reactive scalars," Phys. Fluids **7,** 754–763 (1995).
20. J. Fielding and M. B. Long, "Optical flow velocimetry validation images," http://cld3.eng.yale.edu/fielding.